Chemical Science

Accepted Manuscript

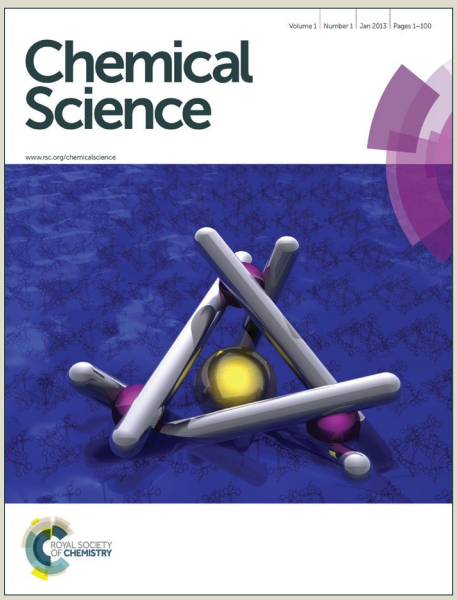

ROYAL SOCIETY OF CHEMISTRY

www.rsc.org/chemicalscience

Journal Name

ARTICLE

Shape-Memory Effect in an Organosuperelastic Crystal

Satoshi Takamizawa*[a] and Yuichi Takasaki[a]

Received 00th January 20xx,
Accepted 00th January 20xx

DOI: 10.1039/x0xx00000x

www.rsc.org/

Shape-memory materials, i.e., polymers (SMPs: shape-memory polymers) and alloys (SMAs: shape-memory alloys), have been developed in very different ways since they are historically far apart in material type as well as physical property. In the deformation process, SMPs require only slight stress due to the properties of organic polymer solids and reveal a smaller recovery force during the thermoplastic process whereas SMAs require relatively large stress due to metallic properties and thermally tighten to generate a larger recovery force by destabilization of the stress-induced phase. An investigation into the unexplored area of the material adjoining both ends of SMPs and SMAs would lead toward a better understanding of shape-memory materials and extend future applications and material types. Here, we report the discovery of a shape-memory effect in an organic crystal bearing a combination of crystal transformability such as in SMAs with organic components like SMPs.

Introduction

Shape-memory materials are fascinating materials that regain their original shapes from mechanically deformed states and are categorized into polymers and metal alloys. The two material types are completely different, not only in type of material but also in the nature of their shape-recovery. Shape-memory polymers[1] (SMPs) are rather flexible and work via thermal relaxation of the polymer to show up their hidden tensility by the positional reversion of embedded linkup or stable bundling points, whereas shape-memory alloys[2] (SMAs) are stiff and transform to gain enough recovery force to overpower stiffness via thermal phase destabilization of the stress-induced domains. Thus, SMP recovery during the thermoplastic process is feeble whereas SMA recovery is powerful with increased tension with a rise in temperature.

After the term “shape memory” appeared during the development of Ni-Ti as an engineering alloy in 1960s,[3] SMAs have been focused upon because of their new properties and anticipated applications. The shape-memory effect is considered as a phenomenon strongly related to superelasticity. The earliest reports on shape memory and superelasticity were made for Au-Cd in 1951[4] and 1932.[5] Despite the advantages of strength and/or durability in applying shear by the operation of tension or compression, metal alloys require a certain amount of energy input to cause deformation. Thus, a certain bias force is needed in the cyclic actuating motion, which causes problems in micro-device applications such as micro springs, micro valves, and microelectromechanical systems (MEMS). Furthermore, materials free of toxic elements are required, especially for medical uses from a biocompatible perspective. The chemical synthesis of SMA-like materials would bring important contribution to evolution of the materials science since the current SMA materials are limited to metal alloys and ceramics.[6]

While the mechanism of the shape-memory effect of SMAs is not fully understood, Otsuka and Shimizu proposed an empirical hypothesis for SMAs[7] that shape-memory effect and superelasticity are fundamentally coexisting phenomena; one phenomenon appears by giving the appropriate temperature if the other phenomenon appears. In particular, the thermoelastic martensitic transformation, which generates the mobile interfaces during the growth of daughter domains by temperature change, is commonly thought to be important for thermomechanical shape-recovery motion, which is so-called shape-memory effect in SMAs.

On the other hand, the term “shape-memory” in polymer science is rather new, appearing in the middle of the 1980s[8] where SMP’s shape recovery occurs during thermal softening around glass transition temperature to release the restraint in shape recovery motion. The shape memory effect involved in SMAs had not been known for any organic materials including SMPs although organic materials do have extendibility in various kinds of polymers in developing functional material chemistry. Thus, we thought that an investigation into the unexplored area of the material adjoining both ends of SMPs and SMAs would lead toward a better understanding of shape-memory materials and extend future applications and material types.

Considering the current situation of SMAs and SMPs, shape-memory materials having both powerful recovery and easy deformation have not yet been identified and there is no such applicable theory for it. While polymers and metals obviously have promising potentials for elastic materials, molecular crystals consisting of organic compounds have not been of much interest because organic crystals seem to be poorly suited for handling mechanical stress.

[a] Department of Nanosystem Science; Graduate School of Nanobioscience; Yokohama City University; 22-2 Seto; Kanazawa-ku, Yokohama, Kanagawa 236-0027; Japan.

†Electronic Supplementary Information (ESI) available: experimental details and crystallographic data. See DOI: 10.1039/x0xx00000x

We have discovered that organic crystals potentially have superelasticity (organosuperelasticity),[9,10] which recoveries their shapes from mechanical deformation with martensitic transformation while some organic and organoionic crystals are known to exhibit shear-induced martensitic transformation without spontaneous shape-recovery properties.[11-14] However, we could not find the shape-memory effect in the organosuperelastic crystals of terephthalamide[9] or 3,5-difluorobenzoic acid,[10] probably due to their poor thermal connection of the mechanical phase. SMAs are known to have the specific thermal phase connection of their superelastic region to twinning region.

Consequently, the requirements for organic material design towards SMA-like behavior would naturally be concerned with the capability of thermal transition under the suppression of a component's diffusion for generating martensitic transformation with the thermally interchangeable superelasticity connected to the lower twinning region without spontaneous restoration characteristics. Furthermore, metal alloys have many compositions and ordered alloys are known to prefer martensitic (non-diffusive) transformation to complicated plastic deformation.

Considering the empirical material and thermal characteristics of SMAs mentioned above, we focused on the relatives of plastic crystals[15] but without transiting into mesophase despite the fact that the plastic deformation derived from the events of easy dislocation and slide could occur due to weak interactions among organic components. We investigated organoionic single crystals consisting of binary molecular components with a spherical shape as similar as possible to the rigid sphere atomic components in metal alloys. Herein, we report the first SMA-like shape-memory effect of organic molecular crystals. The material exhibits powerful shape recovery along with easy deformability.

Results and discussion

The compound is tetrabutyl-*n*-phosphonium tetraphenylborate ($(P^nBu_4)^+(BPh_4)^-$ (**1**)). Its single-crystals were prepared by recrystallization from an acetone solution of crude **1**, which was first obtained as precipitates from a mixed aqueous solution of PBu_4Cl and $NaBPh_4$. While the crystal **1** is soft in terms of 0.88 GPa by Young's modulus at room temperature, similar to high-density polyethylene, **1** exhibits a martensitic transformation rather than a plastic deformation. (Fig. 1) Through application of shear force at room temperature, a colorless rod-shaped crystal (α phase) underwent stress-induced martensitic transformation in growing a twin (α^+/α^- state) with mobile planar phase boundaries across the crystal rod in keeping an invariant bending angle of 12°. Sequential displacement of the shear position on the crystal rod can form zigzag crystals through the use of tweezers under a microscope. By homogeneous warming, the deformed crystal regained its straight shape, showing the thermal shape recovery of **1**. (Fig. 1a) In contrast, applying heat to the straight rod-shaped crystal with a longitudinally thermal gradient bent the crystal by generating a high-temperature phase (β) from the original phase (α). This was done in a quick shifting bending position by regulating the applied heat with a definite bending angle of 6° at the boundary. (Fig. 1b) The practical shape-memory effect of **1** was clearly confirmed by heat sweeping of the deformed crystal specimen with the partial generation of the β phase through the α/β/α transient state. (Fig. 1c)

Single-crystal X-ray diffraction analysis[16] gave the crystal connections under the shear-induced bending state. By warming the crystal **1**, the crystal system changed from triclinic *P*-1 in the α phase (394 K, *V*/*Z*: 960.7 Å^3) into monoclinic $P2_1/n$ in the β phase (403 K, *V*/*Z*: 968.5 Å^3) with a 0.8% expansion by volume. (Table S1) Crystal face indexing showed the interfaces for shear-induced twinning with α^+/α^- ($(103)_{\alpha+}//(103)_{\alpha-}$ and $(-10-3)_{\alpha-}//(-10-3)_{\alpha+}$) and for the heat-induced crystal of $\alpha^{\pm}/\beta$ ($(205)_{\alpha+}//(-3-13)_{\beta}$ and $(205)_{\alpha-}//(3-1-3)_{\beta}$)), respectively. (Figs. 1d & 1e)

Since the neighbouring crystal cells fit exactly on the mirror interface in α^+/α^-, there is no lattice strain at the interface although conformational strain can exist in the component molecules on the interface. In contrast, a certain lattice strain did exist at the α/β interface with the rate of facing crystal surfaces in 0.98 by $S_{(205)\alpha+}/S_{(-3-13)\beta}$.

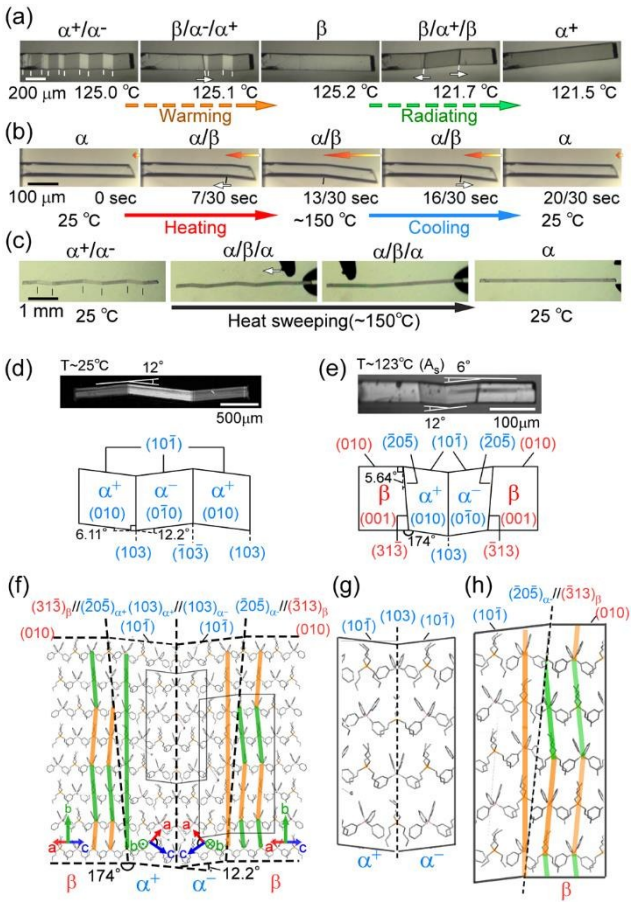

Fig. 1 Thermal shaping recovered the deformed zigzag α^+/α^- prepared at room temperature to the "remembered" straight rod β around 125.0 °C by warming (a); thermal actuation for cyclic α⇄β/α transformation by heat fluctuation with an iron at 150 °C (b); and shape recovery by a heat-sweep over the deformed zigzag pattern of α^+/α^- (c). (Movie S1) Crystal morphology (d-h): photographs taken with a polarized microscope with accompanied crystal face indexes caused by shear at room temperature for α^+/α^- twin (d) and around 123 °C for $\alpha^+/\alpha^-/\beta$ multiphase (e); molecular correspondence at interface estimated by X-ray results ($\beta/\alpha^+/\alpha^-/\beta$ (f), and magnified for α^+/α^- (g) and α^-/β (h)). Color auxiliary lines in (f) and (h) indicate molecular alignments.

Thus, the α and β crystal faces should respectively feel the forces of face extension and contraction, which can generate a certain shear contributing to reverse transformation. The crossing plane angles related to the unit cells from the X-ray data are estimated at 12.2° and 5.3° for α^+/α^- and $\alpha^\pm/\beta$ ($=\alpha^+/\beta$ or α^-/β) connections, respectively, which agree with the crystal bending angles of 12.0° and 6.0° observed under a microscope. This demonstrated how to preserve one-to-one molecular correspondence during transformation to satisfy the martensitic manner. (Refer to Figs. 1d & 1e.) The α^+/α^- takes a rotary reflection plane regarded as a Type II twin,[17] which requires rotation of the molecules when the boundary moves during crystal transformation. The $\alpha^\pm/\beta$ interface has a similar correlation in the α^+/α^- interface. The density of the molecules at the interface should be unchanged in α^+/α^- and its waviness changed along the $\alpha^\pm/\beta$ boundary plane. In the appearance of the $\alpha^\pm/\beta$ interface, the method of deviation of molecular density (orange and green lines in Figs. 1f & h) determines either the interface of α^+/β or α^-/β. Since molecular components have certain complexities in figures unlike the atomic components in SMAs, molecular correspondence at the interface can be regulated by a change of orientation and conformation as well as their relative position. A minimal molecular rotation with a harmonic conformational change can achieve molecular correspondence in the interface without a break in the crystal.

Thermal transition for **1** from the low temperature phase (α) to the high temperature phase (β) was confirmed in DSC measurements. (Table 1, Fig. S3) The transition temperatures and thermodynamic parameters were: $T_{\alpha\text{-}\beta}$= 122.94 °C; ΔH (ΔS)= 3.01 kJ mol^{-1} (7.60 JK^{-1} mol^{-1}) for the transition from α to β phase; T_m= 230.05 °C; ΔH (ΔS)= 41.0 kJ mol^{-1} (81.4 JK^{-1} mol^{-1}) in melting. Because of the sufficiently large ΔS (>20.9 JK^{-1} mol^{-1} [18]) at melting, the β phase should not be considered a plastic mesophase but instead an ordinal crystal phase. Temperature hysteresis can be defined by four pertinent transition temperatures (M_f (T_e for cooling), M_s (T_0 for cooling), A_s (T_0 for heating), and A_f (T_e for heating) were 118.56, 120.46, 123.00, and 124.97 °C, respectively, with respect to the scientific notation for SMAs) with an extremely small separation of 2.5 K between A_s and M_s for **1**. Since interfacial inconsistency increases separation in temperature hysteresis, **1** should have good interfacial consistency, which is preferable to the non-diffusional crystal-to-crystal transformation accompanying crystal phase transition. The α-β thermal structural transition of **1** was confirmed in the PXRD measurements (Fig. S4).

Table 1. Thermodynamic parameters obtained with DSC measurements for **1**.

Phase transition (α to β)			Melting (fusion of β crystal)			Index temperature		
$T_{\alpha\text{-}\beta}$/°C	ΔH/ kJmol^{-1}	ΔS/ $JK^{-1}mol^{-1}$	T_m/°C	ΔH/ $kJmol^{-1}$	ΔS/ $JK^{-1}mol^{-1}$	$A_s(A_f)$/ °C	$M_s(M_f)$/ °C	A_s-M_s / °C
122.94	3.01	7.60	230.05	41.0	81.4	123.00 (124.97)	120.46 (118.56)	2.54

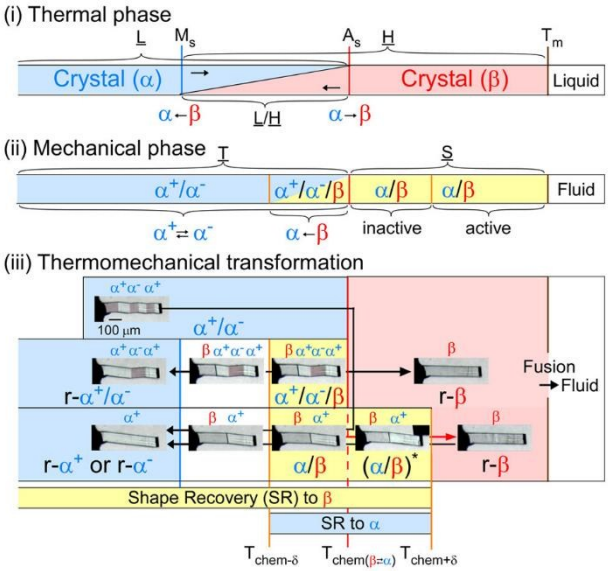

Fig. 2 Phase diagram for **1**: thermal transition (upper), kinetic phase diagram for force-induced mechanical phase (middle), and shape-recovery diagram for thermomechanical transformation (bottom). (M_s, 120.46 °C; A_s, 123.00° C; T_m, 230.05 °C. SR, r-α or r-β mean shape recovery and crystal phase restored into the original shape. *Shear is needed to conserve the deformation.)

From the thermal perspective of the crystal phase of **1**, the crystal phase should be α below M_s (L) and β over A_s (H).(Fig. 2(i)) Either phase is allowed between M_s and A_s (L/H) in the dependence on temperature in going up from α or down from β. We recorded the cyclic strain curves caused by shear on $(10\text{-}1)_\alpha$ and $(010)_\beta$ at various temperatures between –50 °C and 130 °C. Conditions of cyclic shear test on crystal **1** are summarized in Table S2. The kinetic properties can be divided into martensitic twinning (T) and superelastic (S) regions. In the shear-induced transformation of **1** under our experimental condition, T spreads from at least –50 °C to A_s (123 °C) in L. The superelastic region (S) is located from A_s up to at least 129 °C in H. In T, the crystal transformed as $\alpha^+ \rightarrow \alpha^-$ by constant amplitude of shear and left a residual strain. (Fig. 3a) In contrast, the crystal was spontaneously restored above A_s temperature at the beginning of S. (Fig. 3b) The shear for reverse transformation drew cyclic shear-strain curves without residual strain. With a typical plateau, the cyclic curves demonstrated superelasticity (organosuperelasticity[9,10]) during the progress of transformation. The superelastic transformation of **1** was reproduced in 100 cycles of measurements at 124.5 °C. (Fig. S10)

From the shear-strain curves in Figs. 3a & 3b, notation in the shear tests pointed to the typical curve for $\sigma_{\#}$(mother→daughter) (#: nucleation, forward-transformation, reverse-transformation, and chemical). (Fig. 3c) The critical shear for transformation, $\sigma_{f\text{-}trans}$, exhibited a slight decrease with a rather constant amplitude in elevating the temperature from –50 °C up to A_s at which point $\sigma_{f\text{-}trans}(\alpha^+ \rightarrow \alpha^-)$ was replaced with $\sigma_{f\text{-}trans}(\beta \rightarrow \alpha)$ along the thermal change of the mother crystal phase from α to β. (Figs. 4 & S9)

The amplitude of $\sigma_{f\text{-}trans}$ showed a sharp peak of 0.25 MPa around –10 °C, immediately decreased to 0.11 MPa by 20 °C, and then decreased slightly in approaching 0.02 MPa below A_s. Across A_s $\sigma_{f\text{-}trans}$ leaped linearly in temperature with a gradient of

0.135 MPa °C^{-1}. The gradient is known to be related to enthalpy change and rate of strain in the transformation. (4.11 MPa °C^{-1} for the Ti-Ni alloy)[19] (The estimated transformation enthalpy is -3.26 kJ mol^{-1} for **1** using the Clausius-Clapeyron equation.[20]) The amplitude of σ_{nucl} followed the temperature course of $\sigma_{f\text{-}trans}(\alpha^{+}\rightarrow\alpha^{-})$ in a moderate manner and eventually became undetectable after showing a peak by immediately passing A_s. After reaching the S region, superelasticity takes place. The vertical (shear stress) width in shear-strain hysteresis was regarded as constant at 0.123 MPa to depict the parallel lines for $\sigma_{f\text{-}trans}(\beta\rightarrow\alpha)$ and $\sigma_{r\text{-}trans}(\beta\leftarrow\alpha)$. The linear leap of $\sigma_{f\text{-}trans}(\beta\rightarrow\alpha)$ and $\sigma_{r\text{-}trans}(\beta\leftarrow\alpha)$ was launched from almost negligible shear. This means the indexes for superelastic transformation change along with temperature. (Refer to Table S3 & Fig. S11.) For the definition of S, chemical shear ($\sigma_{chem}(\beta\rightleftarrows\alpha)$) should be considered, which is located between $\sigma_{f\text{-}trans}(\beta\rightarrow\alpha)$ and $\sigma_{r\text{-}trans}(\beta\leftarrow\alpha)$. The mean line can be chemical shear (σ_{chem}) because the width of the two lines seems to be sufficiently narrow although the position of σ_{chem} should be shifted by the relationship of the difference in the thermodynamic energy of the crystal phase and, in addition, the loss of energy depending on the way of deformation.

The $\sigma_{chem}(\beta\rightleftarrows\alpha)$ just intercepts A_s at which $T_{chem}(\beta\rightleftarrows\alpha)$ can be defined. This is reasonable since the phase change should cause the chemical evocation of reverse transformation. A_s is the temperature in crossing the Gibbs free energies of the α and β phases while $\sigma_{f\text{-}trans}$ and $\sigma_{r\text{-}trans}$ are expected to intercept at the M_s and A_s temperatures,[21,22] respectively, if the common kinetics correlation is considered, which was proposed for thermomechanical pseudoelasticity in SMAs.[23] From a general view, the observed thermomechanical diagram for **1** is similar to the thermoelastic martensitic transformation for SMAs proposed by Otsuka and Shimizu in 1986.[24]

A more detailed definition is required for the thermomechanical transformation of the shape recovery of **1**. In the temperature range between $T_{f\text{-}trans}(\beta\rightarrow\alpha)$ and $T_{r\text{-}trans}(\beta\leftarrow\alpha)$, which includes a temperature region even lower than A_s, applied force can induce $\beta\rightarrow\alpha$ transformation to be an α/β crystal state without a spontaneously reversing transformation.

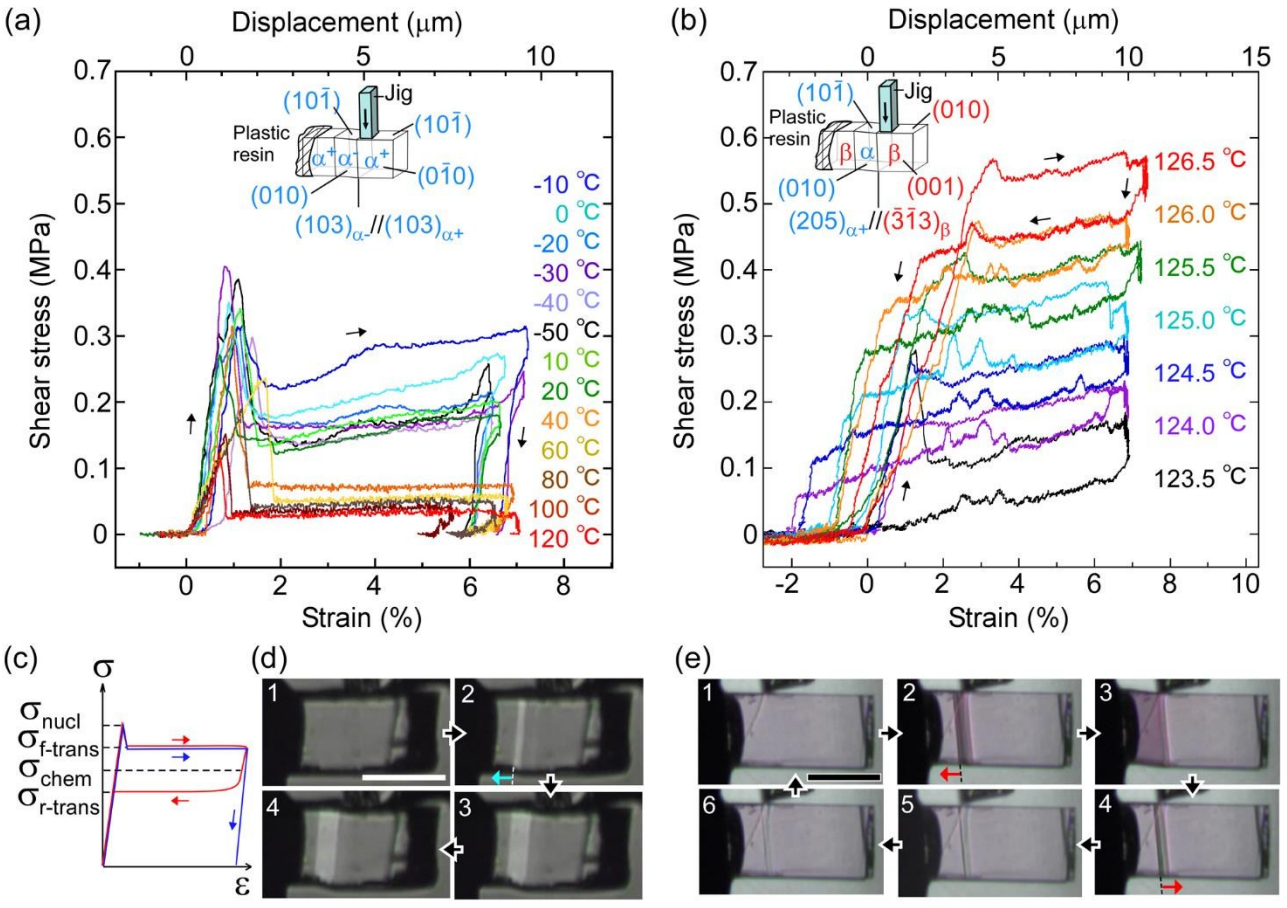

Fig. 3 Shear-strain curves for single crystal **1** at various temperatures: martensitic transformation of twinning α (a) and superelastic β (b) caused by pushing the top surface of the crystal specimen fixed on a hot and cold stage. The experimental conditions are summarized in Table S2, and all stress-strain curves are shown in Fig. S8. In the current shear direction, based on the crystal data, the maximum strain (ε_{max}) is expected for α^{+}/α^{-} at 0.217 and for β/α at 0.107 according to the combination of cells. Schematic curve at lower left shows typical traces for twinning (blue) and superelasticity (red) with the designations of shear used in this paper (c); photographs with a polarized microscope at –10 °C (d) and 126.5 °C (e). (Movie S2)

In considering the allowance of $\alpha^+ \rightarrow \alpha^-$ twinning caused by shear, the static deformed state should be categorized into three temperature parts: α^+/α^- below $T_{chem-\delta}$, $\alpha^+/\alpha^-/\beta$ between $T_{chem-\delta}$ and T_{chem}, and β/α between T_{chem} and $T_{chem+\delta}$. (Refer to Fig. 2(iii).) Thus, the shape-memory region (mechanically deformed state) can take α^+/α^- below A_s (T_{chem}). $\alpha^+/\alpha^-/\beta$ deformation can be prepared between $T_{chem-\delta}$ and T_{chem} and superelastically regains the β solid shape if crossing over $T_{chem+\delta}$ in elevating temperature. The superelastic recovery of the deformed crystal needs a δ rise in temperature against the thermal transition temperature of A_s (T_{chem}). The shape-recovery velocity ($v_{r\text{-}trans}$) in the spontaneously superelastic reverse transformation increases in proportion to the square of temperature as the strength of induced shear increases in relation to $v_{r\text{-}trans} \propto \sigma_{r\text{-}trans}^2$ ($\because \sigma_{r\text{-}trans} \propto (T\text{-}T_{chem+\delta})$), which is suggestive of the conversion of potential energy to kinetic-energy. (Fig. S5) In the heat-induced reversible transformation, the crystal of **1** thermally transforms across the transition temperatures of M_s (β→α) and A_s (α→β) in the manner of an isothermal martensitic transformation. Due to the ease in the interface shuttle in **1**, mere thermal transition can recover shape in generating a slight shear of 0.03 MPa at M_s and less than 0.01 MPa at A_s. (Fig. S9)

The temperature part between $T_{chem-\delta}$ and $T_{chem+\delta}$, which depends on the shear-strain hysteresis, takes the two-way shape-memory region[25] since the mechanical deformation in this temperature rage is capable of recovering α→β and β→α thermal transformation for heating and cooling, respectively.

In order to investigate the thermal replacement of martensitic transformation with crystal breaking under stress, a unidirectional compression test was performed on the $(10\text{-}1)_\alpha$ and $(010)_\beta$ crystal faces, the same direction as in the shear tests. (Fig. 5) The plastic deformation derived from the events of easy dislocation and slide could occur despite organic molecular solids with weak intermolecular interaction. For example, simple ionic crystals such as sodium chloride are known as a typical solid that undergoes plastic deformation.[26]

As the temperature increased, Young's modulus (*E*), which is concerned with the elastic hardness of a solid, changed from 0.5 GPa at –30 °C to a peak of 1.43 GPa at 10 °C, decreased almost linearly to the M_s point with 0.4 MPa, jumped around A_s to show a sudden peak at 130 °C with 0.9 GPa, and finally decreased quickly and approached zero at melting temperature. The yield pressure π_y started at 10 MPa to end at 1 MPa close to the melting point of 230 °C through the highest peak around 10 °C and jumped around 130 °C in the same manner as Young's modulus but in a rather moderate fashion. At the narrow region over A_s just after thermal phase changed from the α to the β crystal phase, Young's modulus and the yield pressure suddenly jumped, resulting in getting a tentative hardness of the β phase crystal with an increase of tolerance to crystal compression against stress.

From the viewpoint of crystal breaks caused by stress, some deformation can occur if a solid yields plastically before martensitic transformation begins. The yielding process should match with the compression pressure π_y on the contact area of the jig (Fig. 3a, b). (Fig. 5a) The crossing point of π_y and nucleation pressure (π_{nucl}) is around 125 °C. Consequently, the crystal breaking of **1** is triggered by local compression on the jig, which determines the border temperature in H. An effective measurement configuration will practically save the wider temperature region of S with a larger jig's contact area.

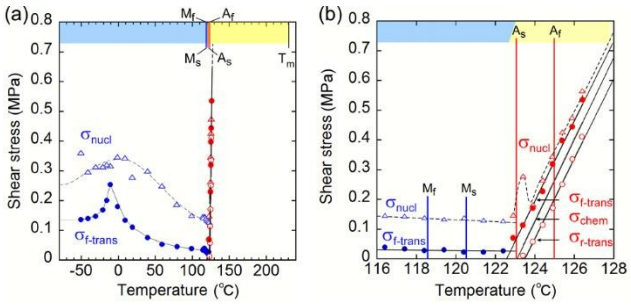

Fig. 4 Temperature dependence of index shears (σ_{nucl} (triangle), $\sigma_{f\text{-}trans}$ (solid circle), and $\sigma_{r\text{-}trans}$ (circle) (σ_{chem} is depicted as a mean line of $\sigma_{f\text{-}trans}$ and $\sigma_{r\text{-}trans}$)): general drawing (a) and extended graph around A_s (b). (Blue and red plots indicate stressed crystal phase for α and β, respectively. Chart upper limb has a color band for indicating phase according to the phase diagram in Fig. 2(ii).) (M_f: 118.56 °C; M_s: 120.46 °C; A_s: 123.00 °C; A_f: 124.97 °C)

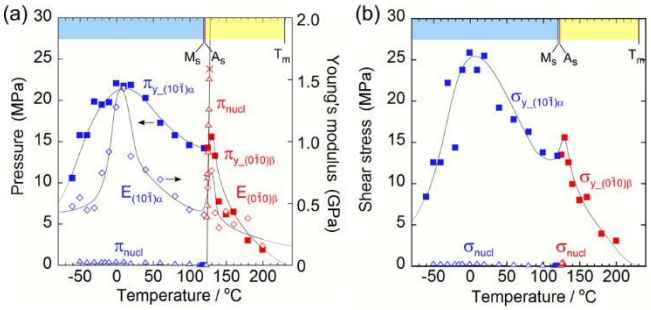

Fig. 5 Comparison of yield stress ($\#_y$) and nucleation stress ($\#_{nucl}$) with respect to pressure (π) on surface (a) and shear (σ) (b). Young's modulus (*E*) is added in the left figure to understand the similarity of *E* to π_y.

Although the crossing of nucleation stress and yield stress in terms of pressure and shear was not observed in L, the crystal seemed to break due to dislocation generation because it broke into mosaic form at around -60 °C whereas it broke in a cleavage manner at around 130 °C.

The thermomechanical characteristics of **1** measured on microcrystals showed easy deformation, less than with SMPs (polyurethane[27]), with a thermal increase of directional recovery shear ($\sigma_{r\text{-}trans}$) up to 10 MPa with 5×10^2 times force back against the twinning shear ($\sigma_{f\text{-}trans}$) of 0.02 MPa below A_s, which is beyond SMAs (Ti-Ni alloy[19]) with 2.6 times that in width, as shown in Fig. 6.

A single crystal of **1** with a 1-cm^2 cross-sectional area is expected to lift a 100 kg weight horizontally with 10 MPa recovery shear generation around 200 °C if the $\sigma_{f\text{-}trans}$ linearly increases in temperature with a gradient of 0.135 MPa $°C^{-1}$ from A_s temperature. In order to visually observe the lifting work, we prepared a large single crystal and cleaved it into a 3.8-cm long specimen of 0.6 g in self-weight with a 0.18 cm^2 (0.6×0.3 cm) cross-sectional area, which had a 1.8-kg lift capability with 1 MPa recovery shear around 130 °C. Considering the current experimental configuration, we hung SUS weighs of 1, 10, and 100 g (more than 10^2 times heavier than the specimen's own weight) with a SUS filament on the single-crystal specimen after the specimen was manually deformed below A_s. After the experimental system was warmed in an oven, the specimen regained its default straight shape by sequential lifting as

the recovery shear increased during the rise in temperature, demonstrating practical and feasible work capability of the shape-memory effect of **1**, (Fig. 7) although the lifting started at 131.0 (1 g), 131.8 (10 g), and 133.4 (100 g) °C, which are higher by 5.9 (131.0-125.1)-8.2 (133.4-125.2) °C than the expected starting temperatures from the microcrystal experiments depicted in Fig. 1a probably due to the non-ideal strain in a large crystal specimen in hanging heavy weights. This demonstrates the desired characteristics of shape-memory materials for miniaturization and conversion of heat into a practical work output within a narrow temperature cycle. It should be noted that **1** exhibits a high A_f point of 124.97 °C, which is higher than 110 °C known as the highest limit for binary Ni-Ti alloys without any additive.

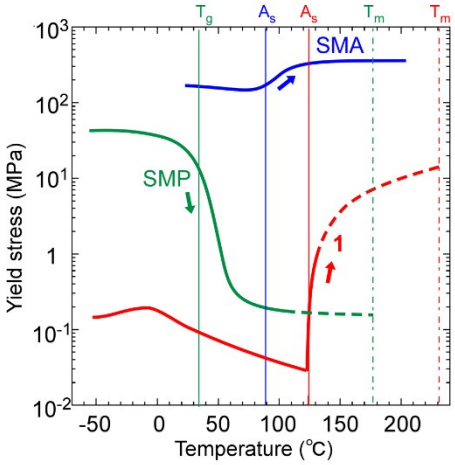

Fig. 6 Comparison of yield stress (or critical shear) of **1** (M_s: 120.46 °C; A_s: 123.00 °C; T_m: 230.05°C) with representative SMP (polyurethane;[27] T_g: 32 °C) and SMA (Ti-Ni alloy;[19] M_s: 75 °C, A_s: 89 °C) (b)

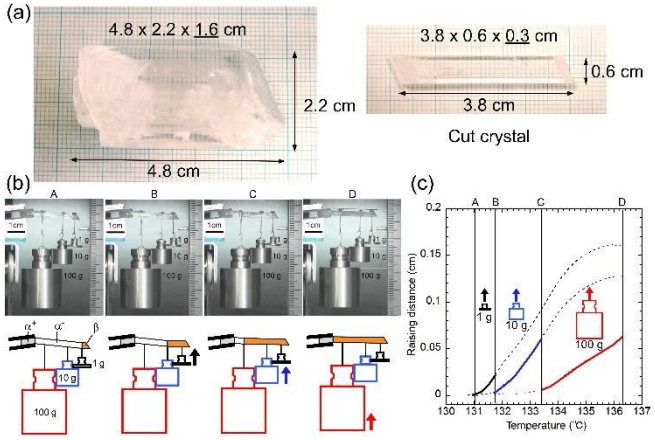

Fig. 7 Photographs of a large single-crystal and a cut crystal for the lifting experiment (a). Snapshots extracted from Movie S3 during the lifting work of **1** hung by 1, 10, 100 g SUS weights in an oven with schematic diagram for the explanation (b) and a sequential lifting course for each weight with temperature rise (c).

Conclusions

In conclusion, we demonstrated a transcendent shape-memory effect in an organic crystal, which can thermally generate a large recovery force in an SMA-like thermal manner with easier deformability than that of SMPs. The thermomechanical properties concealed in organic crystal will at least contribute to the development of new shape-memory (recovery) materials and provide novel strategies for dealing with the current problems in handling conventional SMPs and SMAs for miniaturization, hybridization, biocompatibility, effective thermal work efficiency, and so on. The integrated understanding of shape-memory materials would achieve the augmentation of future applications and material types without being limited to the sciences of polymer chemistry and metal physics.

Experimental

Preparation of materials

Tetrabutyl-*n*-phosphonium tetraphenylborate ($(P^nBu_4)^+(BPh_4)^-$ (**1**)): Two separately prepared 0.15 M aqueous solutions of $NaBPh_4$ and PBu_4Br were mixed at the same volume ratio (equivalent in stoichiometry), immediately precipitating a colorless crystalline powder, which was collected by filtration. After being washed several times with a necessary minimum volume of water, vacuum drying at 25 °C gave a colorless crude powder, which was then recrystallized from acetone or acetonitrile to form colorless crystals in 82.6% yield. Well-formed colorless rod crystals were obtained by recrystallization from acetone and used for the experiments after vacuum drying.

X-ray structural analysis

Single-crystal X-ray structural analysis of **1** was performed at 183, 298, 394, and 403 K on a Bruker Smart APEX CCD area diffractometer (Bruker AXS K.K.) with a nitrogen-flow temperature controller using graphite-monochromated Mo Kα radiation (λ= 0.71073 Å). Empirical absorption corrections were applied using the SADABS program. The structure was solved by direct methods (SHELXS-97) and refined by full-matrix least-squares calculations on F^2 (SHELXL-97) using the SHELX-TL program package. Non-hydrogen atoms were refined anisotropically; hydrogen atoms were fixed at calculated positions using riding model approximation. Crystallographic data of the structure are summarized in Table S1. Crystal face indexing was carried out using SMART in a SHELXTL Ver. 6.12 program package with a twin resolution program.

Thermal analysis

TG-DTA and DSC measurements were carried out on a Shimadzu DTG-60 and DSC-60

Powder X-ray diffraction measurement

PXRD measurements were performed on a Bruker D8 Advance (Bruker AXS K.K.) with a heat controller using Cu Kα radiation (λ= 1.5406 Å).

Stress-strain test

Stress tests were carried out on a universal testing machine (Tensilon RTG-1210, A&D Co. Ltd.) equipped with a microscope and a hot & cold stage. (Fig. S7) After one end of a single crystal was fixed on the metal stage by using plastic resin, a blade-shaped metal jig (5 or 95 μm wide) was pushed across the $(10\text{-}1)_\alpha$ or $(010)_\beta$ surface of the crystal specimen at a constant speed of 200 or 500 μm min^{-1}. (Table S2)

Preparation of bent crystals

The bent crystal specimens were prepared by applying shear stress using tweezers for small crystals under a microscope and fingers for large crystals. (Fig. S13)

Acknowledgements

This work was partially supported by a Research Grant, SUZUKI Foundation, IKEYA Science & Technology Foundation, and Hitachi Metals・Materials Science Foundation (in memory of Kakunosuke Miyashita) for S.T.

Notes and references

1 A. Lendlein, *Shape-Memory Polymers*, Springer-Verlag, Heidelberg, Germany, 2010.
2 K. Otsuka, C. M. Wayman, *Shape Memory Materials*, Cambridge University Press, Cambridge, 1998.
3. W. J. Buehler, J. W. Gilfrich, R. C. Wiley, *J. Appl. Phys*., 1963, **34**, 1475–1477.
4. L. C. Chang, T. A. Read, *Trans*. *AIME*., 1951, **189**, 47–52.
5. A. Ölander, *J. Am. Chem. Soc*., 1932, **54**, 3819–3833.
6. G. Z. Wei, R. Sandstrom, S. Miyazaki, *J. Mater. Sci.*, 1998, **33**, 3743–3762.
7. K. Otsuka, K. Shimizu, *Int. Metals Rev.*, 1986, **31**, 93–114.
8. (a) H. Kimura, F. Teraoka, *J. Osaka Univ. Dent. Sch.*, 1986, **26**, 59-65; (b) C. Liu, H. Qin, P. T. Mather, *J. Mater. Chem.*, 2007, **17**, 1543–1558.
9. S. Takamizawa, Y. Miyamoto, *Angew. Chem. Int. Ed*., 2014, **53**, 6970–6973.
10. S. Takamizawa, Y. Takasaki, *Angew. Chem. Int. Ed*., 2015, **54**, 4815–4817.
11. H. Schwenk, K. Andres, F. Wudl, E. Aharon-Shalom, *J. Phys., Colloq*., 1983, **44**, C3, 1041–1045.
12. T. Ishiguro, T. Ukachi, K. Kato, K. Murata, K. Kajimura, M.Tokumoto, H. Tokumoto, H. Anzai, G. Saito, *J. Phys. Soc. Jpn.*, 1983, **52**, 1585–1592.
13. M. Mukoujima, K. Kawabata, T. Sambongi, *Solid State Commun.*, 1996, **98**, 283-286.
14. F. Kaneko, M. Kobayashi, *J. Phys. Chem. B*, 1997, **101**, 285–292.
15. Some tetra-*n*-alkylammonium salts are known as plastic crystals and are described in A. Xenopoulos, J. Cheng, M. Yasuniwa, B. Wunderlich, *Mol. Cryst. Liq. Cryst. Sci. Technol., Sect. A*, 1991, **214**, 63–79.
16. Crystal data of **1** for the α phase at 183 K (CCDC-1422938): Triclinic, *P*-1, a = 10.1868 (7) Å, b = 18.7141 (13) Å, c = 20.7566 (15) Å, α = 70.748 (2)°, β = 86.972 (2)°, γ = 76.006 (2)°, V = 3623.3 (4) Å^3, Z = 4, D_{calc} = 1.061 Mg m^{-3}, R_1 = 0.0888 (0.2179), wR_2 = 0.1966 (0.2639) for 5053 reflections with $I > 2\sigma(I)$ (for 12760 reflections (21308 total measured)), goodness-of-fit on F^2 = 1.004, largest diff. peak (hole) = 0.724 (-0.349) e Å^{-3}. The α phase at 298 K (CCDC-986256): Triclinic, *P*-1, a = 10.311 (3) Å, b = 18.895 (5) Å, c = 20.770 (6) Å, α = 69.618 (7)°, β = 85.946 (7)°, γ = 76.898 (6)°, V = 3694.1 (18) Å^3, Z = 4, D_{calc} = 1.040 Mg m^{-3}, R_1 = 0.1120 (0.2319), wR_2 = 0.3496 (0.4207) for 4884 reflections with $I > 2\sigma(I)$ (for 12972 reflections (21495 total measured)), goodness-of-fit on F^2 = 1.120, largest diff. peak (hole) = 0.443 (-0.336) e Å^{-3}. The α phase at 394 K (CCDC-986257): Triclinic, *P*-1, a = 10.5582 (11) Å, b = 19.131 (2) Å, c = 20.915 (2) Å, α = 68.892 (2)°, β = 85.501 (3)°, γ = 77.175 (2)°, V = 3842.7 (7) Å^3, Z = 4, D_{calc} = 1.000 Mg m^{-3}, R_1 = 0.0960 (0.2774), wR_2 = 0.2660 (0.3982) for 3496 reflections with $I > 2\sigma(I)$ (for 13522 reflections (22471 total measured)), goodness-of-fit on F^2 = 0.894, largest diff. peak (hole) = 0.421 (-0.264) e Å^{-3}. The β phase at 403 K (CCDC-986258): Monoclinic, $P2_1/n$, a = 12.1401 (14) Å, b = 36.975 (4) Å, c = 17.688 (2) Å, α = 90.00°, β = 102.611 (2)°, γ = 90.00°, V = 7748.1 (15) Å^3, Z = 8, D_{calc} = 0.992 Mg m^{-3}, R_1 = 0.1668 (0.4430), wR_2 = 0.4463 (0.5654) for 3231 reflections with $I > 2\sigma(I)$ (for 19194 reflections (57189 total measured)), goodness-of-fit on F^2 = 1.123, largest diff. peak (hole) = 0.476 (-0.265) e Å^{-3}. CCDC-1422938, 986256-986258 contain the supplementary crystallographic data for this paper. The data can be obtained free of charge from The Cambridge Crystallographic Data Centre via http://www.ccdc.cam.ac.uk/data_request/cif.
17. Y. Murakami, K. Otsuka, S. Hanada, S. Watanabe, *Mater. Sci Eng., A*, 1994, **189**, 191–199.
18. J. Timmermans, *J. Phys. Chem. Solids*, 1961, **18**, 1–8.
19. O. Benafan, R. D. Noebe, S. A. Padula, II, D. J. Gaydosh, B. A. Lerch, A. Garg, G. S. Bigelow, K. An, R. Vaidyanathan, *Scripta Materialia*, 2013, **68**, 571–574.
20. The estimated activated enthalpy for transformation is -3.26 kJ mol^{-1} for **1** using a Clausius-Clapeyron equation ($\Delta H^* = -T_{av}\varepsilon$ ($d\sigma/dT$)) with the values: $d\sigma/dT$= 0.135 × 10^6 Pa K^{-1}; T_{av}= (393.5+396.0)/2=394.8 K; ε = tan(6.11°) × 0.98 (=V_α/V_β) = 0.105; density in β= 0.992 × 10^6 g m^{-3}; and Formula weight= 578.63 g mol^{-1}.
21. K. Otsuka, C. M. Wayman, K. Nakai, H. Sakamoto, K. Shimizu, *Acta. Metall.*, 1976, **24**, 207–226.
22. R. V. Krishnan, L. C. Brown, *Metall. Trans.*, 1973, **4**, 423–429.
23. K. Tanaka, S. Kobayashi, Y. Sato, *Int. J. Plasticity*, 1986, **2**, 59–72.
24. K. Otsuka, K. Shimizu, *Int. Met. Rev.*, 1986, **31**, 93–114.
25. The history and terminology for SMAs: C. M. Wayman, J. D. Harrison, *JOM.*, 1989, **41**, 26–28.
26. R. W. Davidge, P. L. Pratt, *Phys. Status Solidi B*, 1964, **6**, 759–776.
27. S. Farzaneh, J. Fitoussi, A. Lucas, M. Bocquet, A. Tcharkhtchi, *J. Appl. Polym. Sci.,* 2013, **128** (5), 3240–3249.